ARMY RESEARCH LABORATORY

An Optically Based Pressure Measurement Approach for Interior Ballistic Testing

by Michael J. McQuaid

ARL-TR-1472 August 1997

The findings in this report are not to be construed as an official Department of the Army position unless so designated by other authorized documents.

Citation of manufacturer's or trade names does not constitute an official endorsement or approval of the use thereof.

Destroy this report when it is no longer needed. Do not return it to the originator.

Army Research Laboratory
Aberdeen Proving Ground, MD 21005-5066

ARL-TR-1472 **August 1997**

An Optically Based Pressure Measurement Approach for Interior Ballistic Testing

Michael J. McQuaid
Weapons and Materials Research Directorate, ARL

Abstract

This report describes a recent patent disclosure for obtaining an optically based measurement of pressure. The concept, which utilizes pressure-induced changes in polarization to modulate intensity, incorporates a means of addressing a universal shortcoming of optically based techniques—namely, temperature sensitivity. The invention has application for any pressure regime, but will be particularly advantageous for electrically or physically harsh environments. Embodiments of this concept may provide a suitable replacement for piezoelectric-based pressure transducers used in the testing of advanced gun propulsion system concepts. A design for a transducer that could be used to measure pressure from 0 to 1 GPa is provided as an example, and issues related to building a prototype for use in ballistic testing are identified and discussed.

Acknowledgments

The author is grateful to Todd Rosenberger and Joe Colburn for many helpful discussions regarding interior ballistic testing and issues related to pressure measurement techniques.

INTENTIONALLY LEFT BLANK.

Table of Contents

		Page
	Acknowledgments	iii
	List of Figures	vii
1.	Introduction	1
2.	Concept Description	4
3.	Issues in Prototype Development	9
4.	Summary	13
5.	References	15
	Appendix: The Impact of Interference Effects	17
	Distribution List	29
	Report Documentation Page	37

INTENTIONALLY LEFT BLANK.

List of Figures

Figure		Page
1.	Design Concept for an Optically Based Measurement of Pressure: (1) Light Source, (2) Beam Splitter, (3) Polarizer/Analyzer, (4) Temperature-Compensation Media, (5) Pressure-Sensing Media, (6) Reflective Coating, (7) Photocell, (8) Unpolarized Incident Beam, (9) Initial (Linear) Polarization State, (10) Final Polarization State, and (11) Output Beam	5
2.	Pressure-Dependent Intensity Response for Example System With Various Sources: (a) 589-nm Bandpass-Filtered Sodium Lamp and (b) 850-nm SLD	10
3.	Schematic Diagram of Pressure Guage: (1) Pressure-Sensing Media, (2) Temperature-Compensation Media, (3) Polarizer/Analyzer, (4) GRIN Lens, (5) Fiber-Optic, (6) Sealed Diaphragm, (7) Transducer Housing, (8) - Spacers, and (9) SMA Connector	11
A-1.	Plane Wave Propagation in a System of Parallel Dielectric Plates	20
A-2.	Pressure-Dependent Intensity Response for the Example System With a Long Coherence Length, Narrow Band Source at 589 nm	24
A-3.	Pressure-Dependent Intensity Response for the Example System With Antireflection Coatings and a Long Coherence Length, Narrow Band Source at 589 nm	26
A-4.	Pressure-Dependent Intensity Response for the Example System With a Long Coherence Length, Broad Band Source (25-nm FWHM Lorentzian Distribution Centered at 850 nm)	27

INTENTIONALLY LEFT BLANK.

1. Introduction

The measurement of combustion chamber and barrel pressures is a critical aspect of interior ballistic research, with even small errors capable of significantly impacting the establishment of weapon system design criteria, such as weight, effective range, and fatigue life. In the testing of conventional solid propellant gun propulsion systems, piezoelectric-based pressure transducers mounted in grease-filled, stepped gauge ports have provided a reliable, robust means for obtaining pressure data [1]. However, this approach has limited effectiveness in research devoted to understanding novel gun propulsion systems employing liquid propellant or electrothermal chemical (ETC) technology. In these cases, high-frequency (up to 100 kHz) pressure fluctuations are produced, and the stepped gauge port, which is employed for thermal protection, biases the frequency response. Measurement fidelity can be improved by mounting the gauges in "through-ports," but the (expensive) gauges can be damaged by exposure to the harsh environment, and temperature sensitivity becomes an issue. Moreover, piezoelectric gauges are inherently susceptible to electromagnetic interference, making their use in ETC systems problematic.

To overcome these difficulties, optically based pressure measurement techniques have been proposed and tested [2]. The art of measuring pressure via optically based approaches encompasses a variety of concepts in which a light source (with a given intensity, spectral content, phase/coherence, and polarization state) illuminates an optical element or elements whose characteristics change as a function of pressure. The change in these characteristics is exploited to modulate the intensity of the light reflected from or transmitted through the elements, and the change is measured with a photodetector (or detectors). Optically based techniques offer freedom from electrical interference and have the potential for small size, high sensitivity, and high bandwidth response [3]. Also, as opposed to piezoelectric transducers, which can only measure pressure transients, optically based techniques can be used to measure static pressures as well. With this capability, optically based measurements could be advantageous in "closed bomb" or strand burner studies.

One concept for modulating (collected) intensity directly is achieved through the use of a deformable reflective diaphragm [4–6]. In embodiments of this concept, a single fiber or fiber bundle transmits light to the diaphragm, and a second fiber or fiber bundle collects and transmits the reflected light back to the detector. The intensity of the reflected light is a function of the reflectivity and pressure-sensitive shape of the diaphragm. Pressure transducers, based on this approach, are now commercially available and being marketed for use in monitoring cylinder pressures in automobile engines (0–20 MPa). However, they have not proven reliable in interior ballistic testing, with temperature sensitivity and variable system losses being considerable development hurdles [2].

A concept for altering the spectral content of a source to produce an intensity change relies on the pressure-induced changes in the band gap of semiconductor materials [7]. The band gap change produces a shift in the absorption profile of the material, altering the spectral content of light that propagates through it. The change in content is observed as a change in intensity when an appropriate bandpass filter is employed in front of the photodetector. Embodiments of concepts based on pressure-induced changes in optical absorption have yet to be proven viable under harsh operating environments, with temperature sensitivity, again, being a severe development hurdle.

One of the methods that has been demonstrated to produce an intensity variation related to a change in phase utilizes an etalon—a transmissive region bounded by two partially reflective surfaces—as the pressure sensitive optical element [8]. The intensity of light reflected from (and transmitted through) an etalon is understood as a superposition of plane waves, the relative phases of which vary as a function of the wavelength of the light, the angle of incidence of the light upon the etalon, the reflectivity of the etalon surfaces, and the optical pathlength of the transmission region. Changes in the relative phase of these waves caused by a change in the optical pathlength produce a variation in intensity, sometimes referred to as a fringe shift. Embodiments of this (interferometric) concept are typically designed so that a large number of intensity cycles are produced over the pressure range of interest, and the resolution of the technique is given by the pressure/intensity cycle. By counting the number of intensity cycles produced by a pressure transient, the magnitude of the transient can be determined. Because the concept is based on

counting intensity cycles, and not the intensity directly, variable intensity losses in the system are not a significant issue.

Although the principles behind interferometric concepts are well established, and a design based on this approach has been tested in a gun [8], there are several practical limitations to the approach. Interferometry requires single-mode light sources, which, at present, are only achievable with expensive solid state lasers. Moreover, if fiber optics are to be employed in the design, single-mode fibers must be utilized. It is also recognized that the intensity modulation is produced for both increases and decreases in pressure. Thus sophisticated counting techniques must be employed if unambiguous results are to be obtained. Finally, optical pathlengths are a function of temperature, and a viable temperature compensation approach has yet to be proposed. Thus, devices based on interferometric concepts are unlikely to be practical in harsh environments such as ballistic testing.

Another concept that has been demonstrated is based on analyzing the polarization state of light that has propagated through a material subjected to uniaxial stress [9]. When stress is applied to a material in (say) the x-direction, the index of refraction for the x-axis (n_x) increases while the index of refraction for the y-axis (n_y) remains constant. Since the velocity (v) is inversely proportional to the index of refraction ($v = c/n$, where c is the speed of light) light polarized parallel to the x-axis propagates at slower speed than light polarized parallel to the y-axis. This difference produces a phase shift, referred to as stress-induced birefringence, that is proportional to the magnitude of the applied stress and the material thickness. A prism polarizer can be utilized to separate the two (orthogonal) polarization states, and the magnitude (intensity) of each is measured via separate photodetectors. The ratio of the difference in the intensities to the sum of the intensities of the two states is a simple function of the applied stress or pressure, and the function is independent of the intensity of the source. The primary limitations of this approach are that a relatively large number (i. e., 7) of optical components are required for the optical processing (between source and detector), and the optical train is complex and difficult to align. Also temperature-dependent effects are not addressed, and in applications where fiber-optic coupling is desired, at least three fibers must be connected to the sensor head.

The optically based pressure measurement concept described in this report will provide a design basis that overcomes many of the limitations of previously studied concepts. The concept is suitable for sensing both static and transient pressures. Optical processing is achieved with just three inexpensive optical elements that are in an in-line configuration, permitting simplicity and compactness in the mechanical design and minimizing alignment difficulty. The design intrinsically compensates for (slow) ambient temperature changes and can be implemented with an inexpensive light source such as a light-emitting diode (LED) or super luminescent diode (SLD). Optical access to the sensor head for both source transmission and signal collection to the sensor head can be implemented with a single optical fiber.

2. Concept Description

Figure 1 illustrates the disclosed approach. The basic components employed in the concept include: a light source (1) that is coupled into the sensor head, producing an unpolarized beam (8) propagating in the +z-direction; a beamsplitter (2); a polarizer/analyzer (3) in the x-y plane and oriented at $\pi/4$ to the x-axis; a birefringent crystal (4) employed for temperature compensation with its fast (lower index of refraction, n_f) axis oriented parallel to the y axis; and a pressure-sensing birefringent crystal (5) whose slow (higher index of refraction, n_s) axis is aligned parallel to the y-axis, the end of which is coated with a reflective coating (6) to produce specular reflection. A photodetector (7) is utilized to monitor the output intensity (11). The pressure-sensing crystal is mounted such that pressure induces stress in the $-z$-direction. The temperature-compensation crystal is mounted so that it remains unstressed.

The passage of light through a birefringent material produces a phase change ($\Delta\Gamma(\lambda,p)$) between the x and y polarization states, which is a function of the wavelength of the light (λ) and the difference in optical pathlengths of the x and y axes. For a light beam propagating in the z-direction of a space-fixed Cartesian coordinate system, the phase retardation at a static pressure (p), which is generated by a naturally birefringent material whose optical c-axis is oriented in the x-y plane, may be approximated by [10]

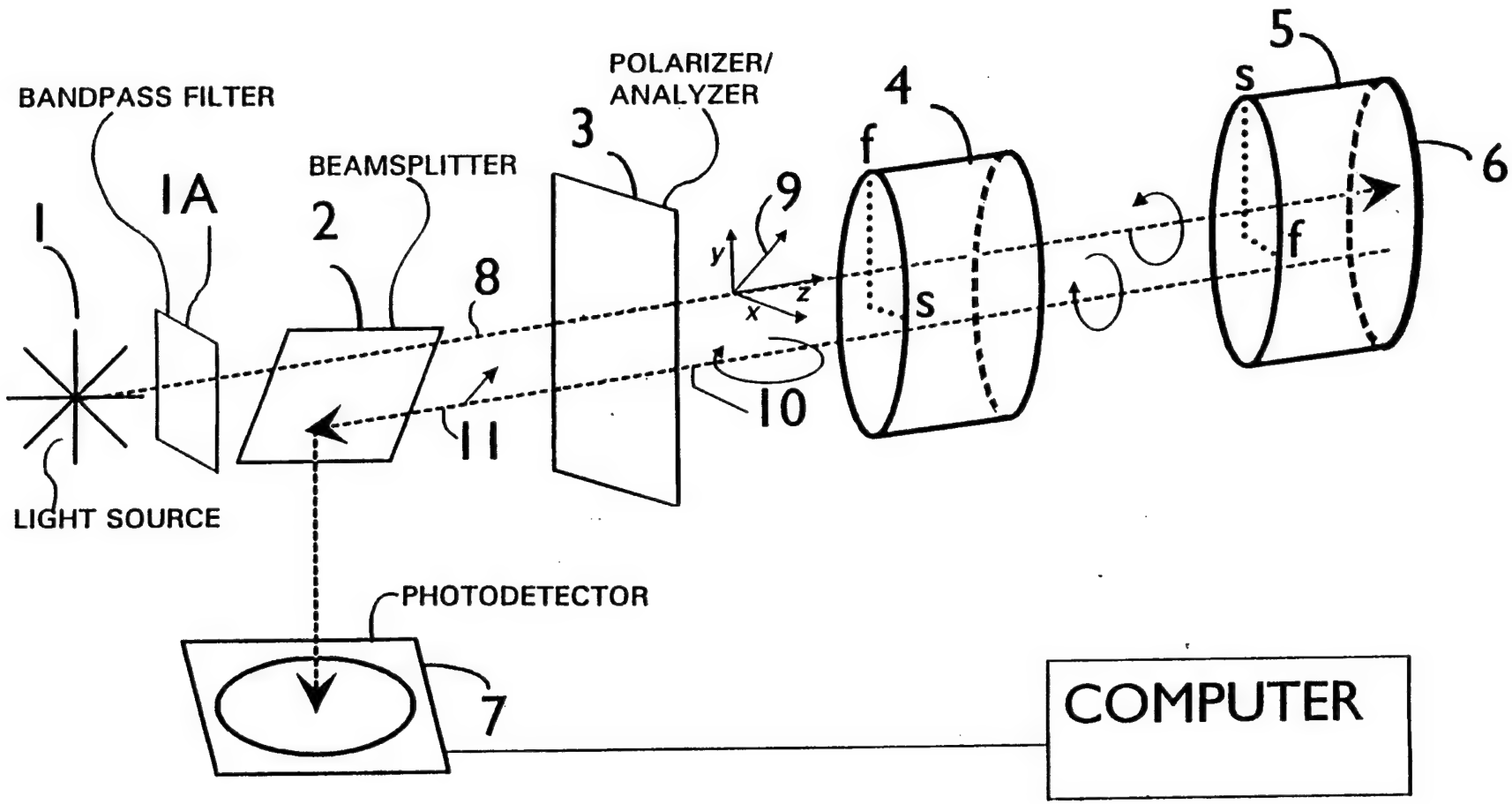

Figure 1. Design Concept for an Optically Based Measurement of Pressure: (1) Light Source, (2) Beam Splitter, (3) Polarizer/Analyzer, (4) Temperature-Compensation Media, (5) Pressure-Sensing Media, (6) Reflective Coating, (7) Photocell, (8) Unpolarized Incident Beam, (9) Initial (Linearly) Polarization State, (10) Final Polarization State, and (11) Output Beam.

$$\Delta\Gamma(\lambda,p) = (2\pi/\lambda)\,(n_f(\lambda,p) - n_s(\lambda,p))\,z(p), \quad (1)$$

where $n_f(\lambda,p)$ and $n_s(\lambda,p)$ are the real part of the pressure- and wavelength-dependent indices of refraction for the fast and slow axes, respectively, and z (p) is the pressure-dependent thickness of the crystal. The wavelength and pressure dependencies of the indices of refraction are the material's dispersion and photoelastic properties, respectively. For the configuration shown in Figure 1, the transmission and reflection back through the pair of crystals produces a phase difference between the x and y axes:

$$\Delta\Gamma(\lambda,p) = (4\pi/\lambda)\,[z_1(p_o)\,(n_f(\lambda,p_o) - n_s(\lambda,p_o)) + z_2(p)\,(n_s(\lambda,p) - n_f(\lambda,p))], \quad (2)$$

where $z_1(p_o)$ is the length of the temperature compensating crystal, $z_2(p)$ is the length of the pressure sensing crystal, p_o is the (ambient) pressure experienced by the temperature sensing crystal and p is the pressure being sensed.

For the case where the crystals are the same thickness (i.e., $z_1(p_o) = z_2(p_o)$) and the pressure-sensing crystal is unstressed, there is no net phase difference produced by propagation through the crystals. Thus, the output beam (10 in Figure 1) remains linearly polarized and oriented at $\pi/4$ to the x-axis. Since it is parallel to the polarizer orientation, it passes unattenuated through it, producing the maximum achievable output intensity for the given system. However, as pressure is applied to the sensing crystal, a phase change is produced that is a function of the compressibility and photoelastic properties of the crystal. Phase differences between 0 and 2π produce elliptically polarized light that has a component orthogonal to the polarizer orientation. Since this component is attenuated by the polarizer, the intensity of the beam incident on the detector is less than in the unstressed case. If the pressure-sensing crystal is stressed such that the phase difference equals π, corresponding to a $\lambda/2$ difference in the optical pathlengths for the x and y axes, the output beam will be linearly polarized orthogonal to the polarizer orientation, and thus completely attenuated by it. (At this point the crystals constitute a 1/4 wave plate, and the system is analogous to a Faraday optical isolator.) With an appropriate selection of crystal thickness and source wavelength, the response between the intensity minimum ($\Gamma = \pi$) and maximum ($\Gamma = 0$) can be customized to give

a single-valued function for the pressure range of interest. In alternate designs, the pressure-sensing crystal may be prestressed, or its thickness relative to the temperature compensation crystal chosen, such that zero intensity corresponds to zero pressure, or to a value that optimizes the response for a given pressure range. Temperature sensitivity is minimized since phase changes induced by thermal expansion (or contraction) of the pressure-sensing crystal are compensated for by an equal and opposite phase change in the crystal, which is not subjected to pressure. (This is analogous to the design of zero-order waveplates.)

To provide a more quantitative picture of the intensity modulation produced by a change in pressure, and demonstrate the potential for building a transducer for use in ballistic testing, the following example is provided. For this example, the birefringent media are chosen to be sapphire crystals that have been cut and polished into windows of identical thickness ($z_1(p_o) = z_2(p_o) = z(p_o) = 5$ mm) and with the optical c-axis parallel to the plane of the window surfaces. The indices of refraction, photoelastic constants, dispersion, and compressibility of sapphire have been measured, and are well behaved over a wide pressure range [11–13]. As a first case, the light source is chosen to be a sodium vapor lamp that is bandpass-filtered to attenuate all but the D-line emission at $\lambda = 589$ nm. (A lamp is not an optimum choice for a practical device, an LED or SLD being preferable, but its monochromaticity is convenient for this example.)

The change in phase produced by a change in pressure is

$$\frac{\partial \Gamma(\lambda,p)}{\partial p} = \frac{4\pi}{\lambda}\left(z\frac{\partial (n_s(\lambda,p) - n_f(\lambda,p))}{\partial p} + (n_s(\lambda,p) - nf(\lambda,p))\frac{\partial z(p)}{\partial p}\right). \qquad (3)$$

Sapphire is naturally birefringent and has high internal transmittance from 200 to 6,000 nm. Values for $n_f(\lambda,p_o)$ and $n_s(\lambda,p_o)$ at 589 nm are 1.760 and 1.768, respectively [11]. To a first approximation, the off-diagonal stress-optic constants are negligible, and thus, $\partial (n_f(\lambda,p) - n_s(\lambda,p))/\partial p$ is approximately zero for the case of uniaxially applied stress [12]. For volumetrically applied stress, this term may be significant. An expression for $\partial z/\partial p$ ($-z/379.3$ GPa) may be derived from the

reported compressive modulus ($z\,\partial p/\partial z = -379.3$ GPa) [13]. Substituting these values into equation (3) and integrating yields

$$\Delta\Gamma = \frac{4\pi}{\lambda}\left(n_s(\lambda,p) - n_f(\lambda,p)\right)\Delta z \tag{4}$$

and

$$\Delta\Gamma = \frac{4\pi}{0.589}(0.008)\left[(5000)\left(1 - \exp\left(\Delta p/379.3\right)\right)\right], \tag{5}$$

where Δz is the change in thickness in microns, and Δp is the change in pressure ($p - p_o$) in GPa.

If external losses (reflections at ambient-crystal interfaces), internal losses (crystal absorption), and interference effects are negligible, the output intensity ($I_o(\lambda,p)$) for the configuration is

$$I_o(\lambda,p) = I_i(\lambda)\left(0.5 + 0.5\cos\left(\Delta\Gamma(\lambda,p)\right)\right), \tag{6}$$

where $I_i(\lambda)$ is the wavelength distribution of the incident beam. The detected output is obtained by integrating with respect to wavelength

$$I_o(p) = \int w(\lambda) I_i(\lambda)\left(0.5 + 0.5\cos\left(\Delta\Gamma(\lambda,p)\right)\right) d\lambda, \tag{7}$$

where $w(\lambda)$ is a weighting factor related to the wavelength sensitivity of the detection system. Integration of equation 7 with $I_i(\lambda)$ equal a delta function at 589 nm and $w(\lambda)$ equal a constant yields

$$I_o(p) = 0.5 + 0.5\cos\left(271.65\pi\left(1 - \exp\left(\Delta p/379.3\right)\right)\right), \tag{8}$$

which, for $\Delta p \ll 379.3$ GPa, is approximately

$$I_o(p) = 0.5 + 0.5\cos(-0.716\pi\Delta p). \quad (9)$$

This function, which is shown in Figure 2(a), is single valued for Δp from 0–1.4 GPa. However, it would not be advisable to employ such a design in experiments in which values approaching 1.4 GPa are expected, since the reduction in dI/dp for pressures approaching this limit raise concerns about accuracy, and pressures above 1.4 GPa will produce ambiguous values.

It is also instructive to consider the response produced by this system when a SLD is used in lieu of the bandpass-filtered sodium lamp. For this example, the spectral distribution of the source ($I_i(\lambda)$) is modeled based on literature values for the output of an Anritsu SD1S101C. This SLD, which is considered representative of such sources, emits a relatively broadband spectrum centered at 850 nm and has a distribution, which (for convenience here) is approximated as a Lorentzian function with a full width half maximum value of 25 nm. The coherence length of this SLD is approximately 100 μm, a value much smaller than the dimensions of the crystals, precluding the possibility of interference effects. Substituting appropriate values into equations (4) and (6) and numerically integrating equation (7) with $w(\lambda)$ equal to a constant yields the response shown in Figure 2(b). It is noted that 850 nm is near the peak of sensitivity of a silicon photodiode, and that for the wavelength range spanning over 99% of the SLD output (50 nm), $w(\lambda)$ = constant is a reasonable approximation. The comparison of Figure 2(a) and (b) shows the influence of wavelength in tailoring a design for a given pressure range, and demonstrates the viability of using a broadband source.

3. Issues in Prototype Development

Although the conceptual basis for designing a transducer whose output is a well-defined function of the pressure is straightforward, there are several optical and mechanical issues that will need to be addressed when building a prototype. One consideration is the desire to mount the transducer in ports designed for standard piezoelectric gauges in ballistic testing. Figure 3 shows a scaled schematic diagram of a sensor head that satisfies this objective. The optical elements include the

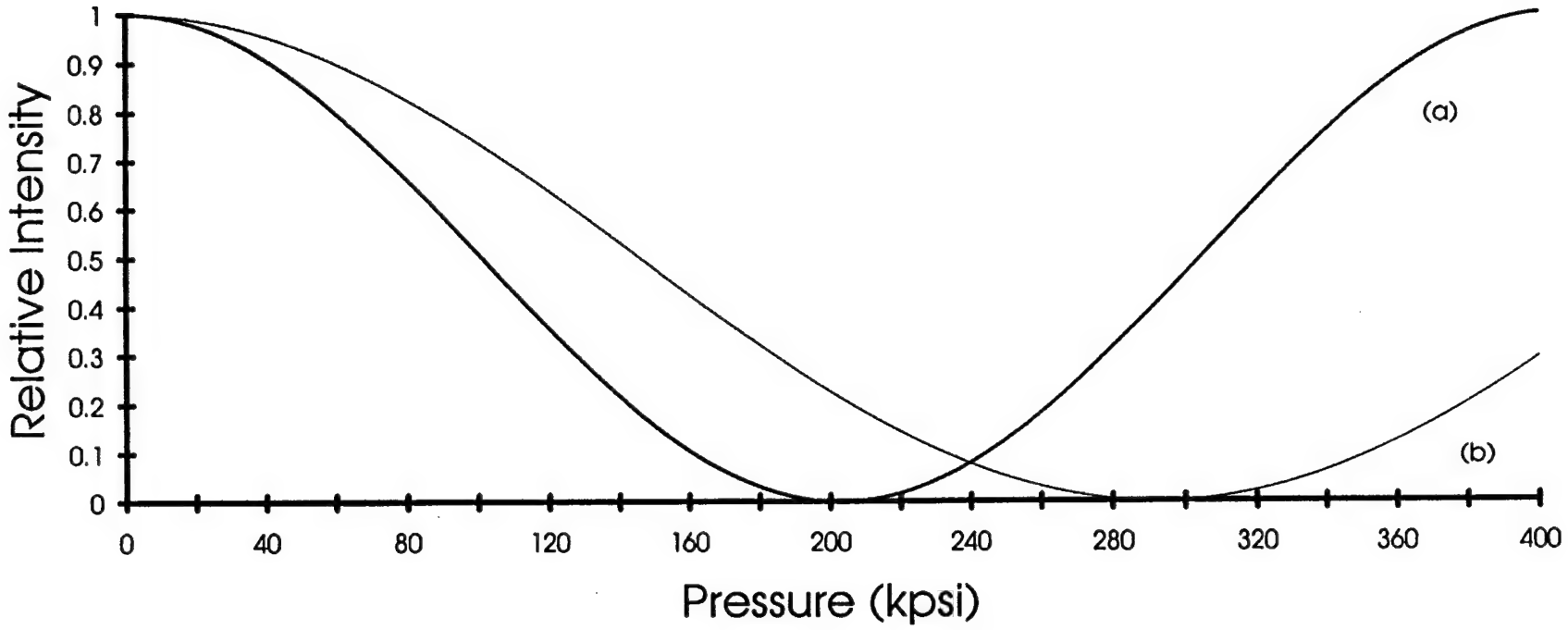

Figure 2. Pressure-Dependent Intensity Response for Example System With Various Sources: (a) 589-nm Bandpass-Filtered Sodium Lamp and (b) 850-nm SLD.

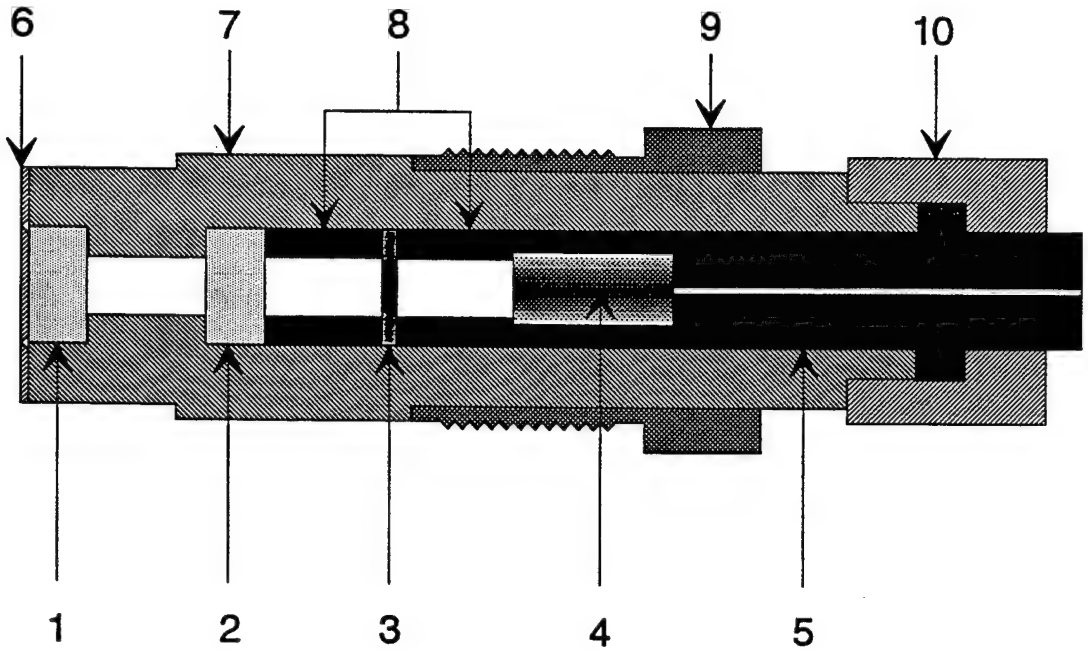

Figure 3. Schematic Diagram of Pressure Gauge: (1) Pressure-Sensing Media, (2) Temperature-Compensation Media, (3) Polarizer/Analyzer, (4) GRIN Lens, (5) Fiber-Optic, (6) Sealed Diaphragm, (7) Transducer Housing, (8) - Spacers, and (9) SMA Connector.

pressure-sensing crystal (1), a temperature compensation crystal (2), a polarizer/analyzer (3), and a gradient index (GRIN) lens (4), which collimates the output of an optical fiber (5). Mechanical components include a diaphragm (6) to protect the reflective coating and ensure a seal of the sensor housing (7). Optically black spacers (8) are employed to reduce spurious reflections and facilitate mounting of the polarizer and collimating lens. The housing is secured to the chamber wall via a threaded sleeve. To facilitate connecting the optical fiber to the transducer head housing, an SMA terminator (10) can be employed. To obtain the most effective collimation of light, the diameter of the fiber should be as small as practical.

One of the problems encountered in the testing of optically based designs has been intensity fluctuations due to cable whip induced by the recoil of the gun. This problem can be avoided in the present design by employing a module that integrates the source and detector and is mounted on the

gun. Such modules can be readily constructed from "commercial, off-the-shelf" components, and "chip-sized" packages, which integrate these functions and are becoming commercially available.

Concerns related to the assumptions employed in deriving equation (8) need to be noted. One is the fact that there will be a certain amount of reflection from each crystal-air interface and losses at the reflecting surface. Antireflection coatings are effective, even for relatively short coherence length sources, and should be employed when feasible. The reflective coating (7, Figure 1) should be chosen to maximize reflected intensity. For this purpose, gold or silver are two of many possible appropriate choices [14]. Equation (8) is also based on the assumption that the light incident on the polarizer is plane parallel, and that the polarizer is "perfect"—i.e., 100% transmission for the polarization state aligned with the polarizer, 100% extinction for the polarization state aligned orthogonal to it. Thus, the relationship of I_o vs. p given in equation (8) will only be a rough approximation. The actual relationship will need to be established through calibration.

Interference effects pose a potential problem if the coherence length of the source radiation is greater than the thickness of the crystals. Being low-cost, compact, and efficient, LEDs, SLDs, and laser diodes are desirable as light sources. The coherence length of these devices are reported to be short, and they should prove useful in this application. But there may be designs where such effects need to be considered. This matter is treated in the appendix. As shown there, antireflection coatings can greatly reduce interference-based intensity modulation.

A more difficult issue to address at this juncture pertains to the mounting of the pressure-sensing crystal. As envisioned in Figure 3, the application of large stresses will almost certainly lead to flexing of the crystal. Not only does this have the potential to introduce nonnegligible, off-axis, stress-optic contributions, it will also produce beam-steering effects. Again, this issue can be addressed through calibration, but, clearly, the design would benefit from a supporting finite element analysis of proposed mount configurations. An issue that is not resolved by the current approach is the relief of the preload on the crystal (stack) caused by thermally induced expansion of the housing. This relief causes an error in peak pressure measurements. Variations of the current approach will be investigated to address this issue.

Finally, although the design should be more rugged than standard piezoelectric designs, it will probably still be necessary to incorporate a thermal barrier into a design, such as Figure 3, in order to protect the reflective coating and reduce temperature gradients produced during a ballistic cycle. Designs that will reduce or eliminate the need or influence of such protection are being considered. One possibility is the use of retardation plates made from polymers. Such plates are on the order of 3 μm thick (for a true zero-order 1/4 wave plate) and are (presumably) much more compressible than typical birefringent media such as sapphire, quartz, and calcite. Thus, some of the potential problems associated with mounting relatively incompressible crystals (which necessitates that they be relatively thick in order to get an appreciable pressure-induced pathlength change) may be alleviated. For example, the polymer can be mounted on a transparent, nonbirefringent, "hard" medium and the pressure stepped down to avoid flexure problems. Moreover, the use of thin plates will reduce the impact of temperature gradients.

4. Summary

This report provides an overview of a recent disclosure for making optically based static and dynamic pressure measurements. The invention employs a sensor head, consisting of a polarizer, and two naturally birefringent media—one of which is responsive to pressure changes and has a reflective coating, and the other which facilitates temperature compensation—producing a modulation of the reflected intensity that is a function of the applied pressure. A design for a transducer that would be suitable for measuring pressures from 0–1 GPa is provided as an example.

INTENTIONALLY LEFT BLANK.

5. References

1. Rosenberger, T. E., J. W. Colburn, and C. R. Ruth. "Pressure Transducer Performance and Measurement Trade-Offs in a Transient, High Temperature Combustion Environment." ARL-TR-914, U.S. Army Research Laboratory, Aberdeen Proving Ground, MD, December 1995.

2. Walton, W. S. "A Special Study of Improvement and Validation of Transducer (Chamber Pressure Measurement). CSTA-7356, U.S. Army Combat Systems Test Activity, Aberdeen Proving Ground, MD, November 1992.

3. E. Udd. "An Overview of Fiber-Optic Sensors." *Review of Scientific Instruments*, vol. 66, p. 4015, 1995.

4. Pahler, R. H., and A. S. Roberts. "Design of a Fiber-Optic Pressure Transducer." Transactions of the ASME, *Journal of Engineering for Industry*, 75-WA/DE-8, 1975.

5. Ho, C. -M. "Optical Pressure Transducer with Randomly Distributed Fiber Optics." U.S. Patent No. 4,158,310, 1979.

6. Liu, H.-T., R. C. Lilley, R. F. Johnson, A. C. Mueller, and R. A. Srnsky. "A Fiber-Optic Pressure Transducer for Measurements in Gun Chambers." *Phase II Final Report* for Contract No. DAAD05-92-C-0215, 1995.

7. Nelson, A. "Fiber-Optic Chamber Pressure Transducer." *Phase I Final Report* for Contract No. DAAD05-91-C-0042, 1991.

8. Steele, T. R. "Interferometric Optical High-Pressure Sensor," BRL-CR-681, U.S. Army Ballistic Research Laboratory, Aberdeen Proving Ground, MD, 1992.

9. Geo-Centers, Inc., "Fiber Optic Chamber Pressure Transducer." *Phase I Final Report* for Contract No. DAAD05-91-C-0123, 1992.

10. Holmes, D. A. "Exact Theory of Retardation Plates." *Journal of the Optical Society of America,* vol. 54, p. 1,115, 1964.

11. Malitson, I. H. "Refraction and Dispersion of Synthetic Sapphire." *Journal of the Optical Society of America* vol. 52, p. 1,377, 1962.

12. Davis, T. A., and K. Vedam. "Photoelastic Properties of Sapphire (-Al_2O_3)." *Journal of Applied Physics*, vol. 38, p. 4,555, 1967.

13. Crystal Systems, Inc. *HEM Sapphire Brochure*, 1990.

14. Haas, G., and L. Hadley. "Optical Properties of Metals." *The Handbook of Optics*, pp. 6–118, W.G. Driscoll (ed.), McGraw-Hill, NY, 1976.

Appendix:

The Impact of Interference Effects

INTENTIONALLY LEFT BLANK.

The analysis presented in section 2 is based on employing an incoherent light source. Although the coherence length of light-emitting diodes (LEDs), super luminescent diodes (SLDs), and laser diodes is short, relative to the component dimensions of the example in section 2, there may be designs where the coherence length is nonnegligible, and interference effects need to be considered. For example, designs could conceivably be based on polymer retardation plates only 3 μm thick. In order to address the ramifications of interference, a model was developed to characterize plane wave transmission through a system of successive dielectric parallel plates. The theoretical approach reported here follows that employed by Jacob's et al. for the case of a single plate bounded by air.[1] Referring to Figure A-1, the solutions satisfying Maxwell's electromagnetic field equations for plane wave propagation ($e^{i\omega t}$) are,

$$\epsilon_{iy} = E_i e^{-\gamma_i z} + E_{-i} e^{+\gamma_i z} \tag{A-1}$$

and

$$H_{ix} = -(\gamma_i / i\omega\mu)(E_i e^{-\gamma_i z} - E_i e^{+\gamma_i z}), \tag{A-2}$$

where μ is the permeability constant, γ_i is the propagation constant ($(2\pi/\lambda)$ (k + in) with index of refraction n and absorption coefficient k) in the i^{th} medium, and E_i and E_{-i} are the amplitude factors for the forward and reverse directions, respectively. The amplitude factors are determined by solving the set of equations corresponding to the requirement that the tangential ϵ and H fields be continuous at each interface. That is, at z_i,

$$E_i + E_{-i} = E_{(i+1)} + E_{-(i+1)} \tag{A-3}$$

and

$$-\gamma_i E_{-i} + \gamma_i E_i = \gamma_{(i+1)} E_{(i+1)} - \gamma_{(i+1)} E_{-(i+1)}. \tag{A-4}$$

---

[1] H. Jacobs, D. A. Holmes, L. Hatkin, and F.A. Brand. " Maximum Gain for Forward–and Backward–Wave Optical Maser Amplifiers." *Journal of Applied Physics*, vol 34, p. 2617, 1963.

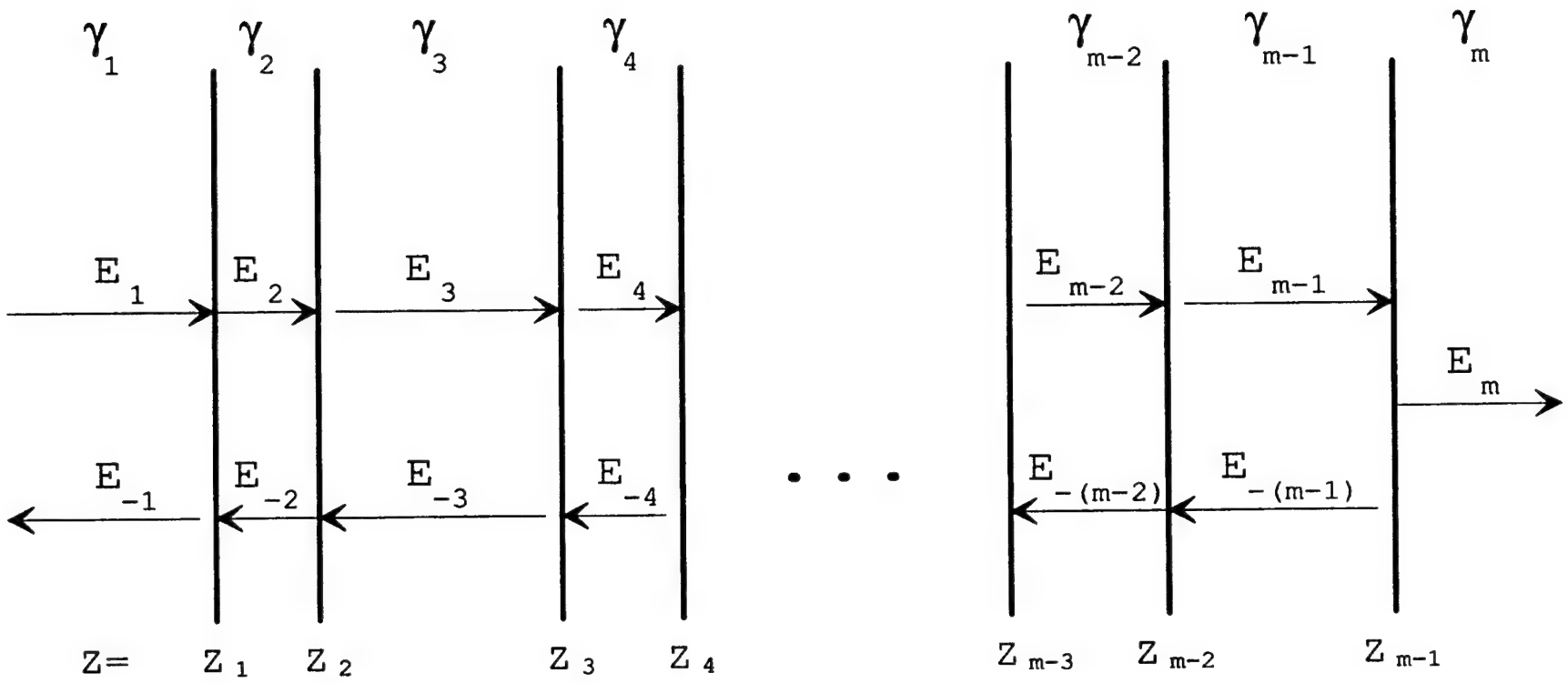

Figure A-1. Plane Wave Propagation in a System of Parallel Dielectric Plates.

The set of equations for a set of (m - 2) plates with thicknesses $(z_i - z_{i-1})$ may be solved via Kramer's method. The amplitude factor for the reflected wave (E_{-1}) is

$$E_{-i} = \frac{\begin{vmatrix} e^{-\gamma_1 z_1} & -e^{-\gamma_2 z_1} & -e^{\gamma_2 z_1} & 0 & 0 & \cdots & 0 & 0 & 0 \\ -\gamma_1 e^{-\gamma_1 z_1} & -\gamma_2 e^{-\gamma_2 z_1} & \gamma_2 e^{+\gamma_2 z_1} & 0 & 0 & \cdots & 0 & 0 & 0 \\ 0 & e^{-\gamma_2 z_2} & e^{+\gamma_2 z_2} & -e^{-\gamma_3 z_2} & -e^{+\gamma_3 z_2} & \cdots & 0 & 0 & 0 \\ 0 & \gamma_2 e^{-\gamma_2 z_2} & -\gamma_2 e^{+\gamma_2 z_2} & -\gamma_3 e^{-\gamma_3 z_2} & \gamma_3 e^{+\gamma_3 z_2} & \cdots & 0 & 0 & 0 \\ 0 & 0 & 0 & e^{-\gamma_3 z_3} & e^{+\gamma_3 z_3} & \cdots & 0 & 0 & 0 \\ \cdot & & & & \cdot & & \cdot & & \cdot \\ \cdot & & & & \cdot & & \cdot & & \cdot \\ \cdot & & & & \cdot & & \cdot & & \cdot \\ 0 & 0 & 0 & 0 & 0 & \cdots & e^{-\gamma_{n-1} z_{n-1}} & e^{+\gamma_{n-1} z_{n-1}} & e^{-\gamma_n z_{n-1}} \\ 0 & 0 & 0 & 0 & 0 & \cdots & \gamma_{n-1} e^{-\gamma_{n-1} z_{n-1}} & -\gamma_{n-1} e^{+\gamma_{n-1} z_{n-1}} & \gamma_n e^{-\gamma_n z_{n-1}} \end{vmatrix}}{\begin{vmatrix} e^{+\gamma_1 z_1} & -e^{-\gamma_2 z_1} & -e^{+\gamma_2 z_1} & 0 & 0 & \cdots & 0 & 0 & 0 \\ -\gamma_1 e^{+\gamma_1 z_1} & -\gamma_2 e^{-\gamma_2 z_1} & \gamma_2 e^{+\gamma_2 z_1} & 0 & 0 & \cdots & 0 & 0 & 0 \\ 0 & e^{-\gamma_2 z_2} & e^{+\gamma_2 z_2} & -e^{-\gamma_3 z_2} & -e^{+\gamma_3 z_2} & \cdots & 0 & 0 & 0 \\ 0 & \gamma_2 e^{-\gamma_2 z_2} & -\gamma_2 e^{+\gamma_2 z_2} & -\gamma_3 e^{-\gamma_3 z_2} & \gamma_3 e^{+\gamma_3 z_2} & \cdots & 0 & 0 & 0 \\ 0 & 0 & 0 & e^{-\gamma_3 z_3} & e^{+\gamma_3 z_3} & \cdots & 0 & 0 & 0 \\ \cdot & & & & \cdot & & \cdot & & \cdot \\ \cdot & & & & \cdot & & \cdot & & \cdot \\ \cdot & & & & \cdot & & \cdot & & \cdot \\ 0 & 0 & 0 & 0 & 0 & \cdots & e^{-\gamma_{n-1} z_{ni-1}} & e^{+\gamma_{n-1} z_{n-1}} & e^{-\gamma_n z_{n-1}} \\ 0 & 0 & 0 & 0 & 0 & \cdots & \gamma_{n-1} e^{-\gamma_{n-1} z_{n-1}} & -\gamma_{n-1} e^{+\gamma_{n-1} z_{n-1}} & \gamma_n e^{-\gamma_n z_{n-1}} \end{vmatrix}}.$$

While the calculation of the determinants can be accomplished by brute force, it proved useful to develop a numerical scheme to calculate the ratio E_{-1}/E_1. This method is as follows. The ratio is defined in terms of two functions,

$$\frac{E_{-1}}{E_1} = \frac{F^N_{m-1}(A)}{F^D_{m-1}(A)}, \tag{A-5}$$

where the functions in the numerator ($F^N(A)$) and denominator ($F^D(A)$) are computed in an iterative manner by (1) setting $z_1 = 0$; (2) specifying the first term in each iteration,

$$F^N_1(A) = \gamma_1 - \gamma_2 \tag{A-6}$$

and

$$F^D_1(A) = \gamma_1 + \gamma_2; \tag{A-7}$$

(3) introducing two other functions ($F^N(B)$ and $F^D(B)$) whose first terms are

$$F^N_1(B) = \gamma_1 + \gamma_2 \tag{A-8}$$

and

$$F^D_1(B) = \gamma_1 - \gamma_2; \tag{A-9}$$

and (4) calculating succeeding terms using

$$F_i(A) = (\gamma_i + \gamma_{i+1}) F_{i-1}(A) e^{\gamma_i(z_1 - z_{i-1})} + (\gamma_i - \gamma_{i+1}) F_{i-1}(B) e^{-\gamma_i(z_1 - z_{i-1})} \tag{A-10}$$

and

$$F_i(B) = (\gamma_i - \gamma_{i+1}) F_{i-1}(A) e^{\gamma_i(z_1 - z_{i-1})} + (\gamma_i + \gamma_{i+1}) F_{i-1}(B) e^{-\gamma_i(z_1 - z_{i-1})}. \tag{A-11}$$

The ratio of (complex) amplitudes can then be used to determine the intensity of the reflected wave (I_{-1j}) relative to the incident wave (I_1) for each axis (j),

$$\frac{I_{-1j}}{I_1} = \left|\frac{E_{-1j}}{E_1}\right|^2 = \left|\frac{a+ib}{a'+ib'}\right|^2, \tag{A-12}$$

and the required phase information

$$\Gamma_j = \tan^{-1}\frac{a}{b} - \tan^{-1}\frac{a'}{b'}. \tag{A-13}$$

The phase shift for propagation along the x and y axes may be computed in this fashion, and the total phase difference is

$$\Delta\Gamma = \Gamma_y - \Gamma_x. \tag{A-14}$$

The intensity observed at the photodetector is then

$$I_R = 0.25^* (E_{-1x}^2 + E_{-1y}^2) + 0.5E_{-1x}E_{-1y}\cos(\Delta\Gamma), \tag{A-15}$$

and the system response may be computed as in equation (7).

To demonstrate the potential impact of interference effects, the example system detailed in section 2 was modeled based on this derivation, and coupled to a nonlinear least-squares-fitting routine to provide optimization capability. As a first case, the results for a long coherence length source whose wavelength distribution is delta function at 589 nm is shown in Figure A-2. The strong fringe pattern is typical of interferometric systems—behavior that is undesirable in this context.

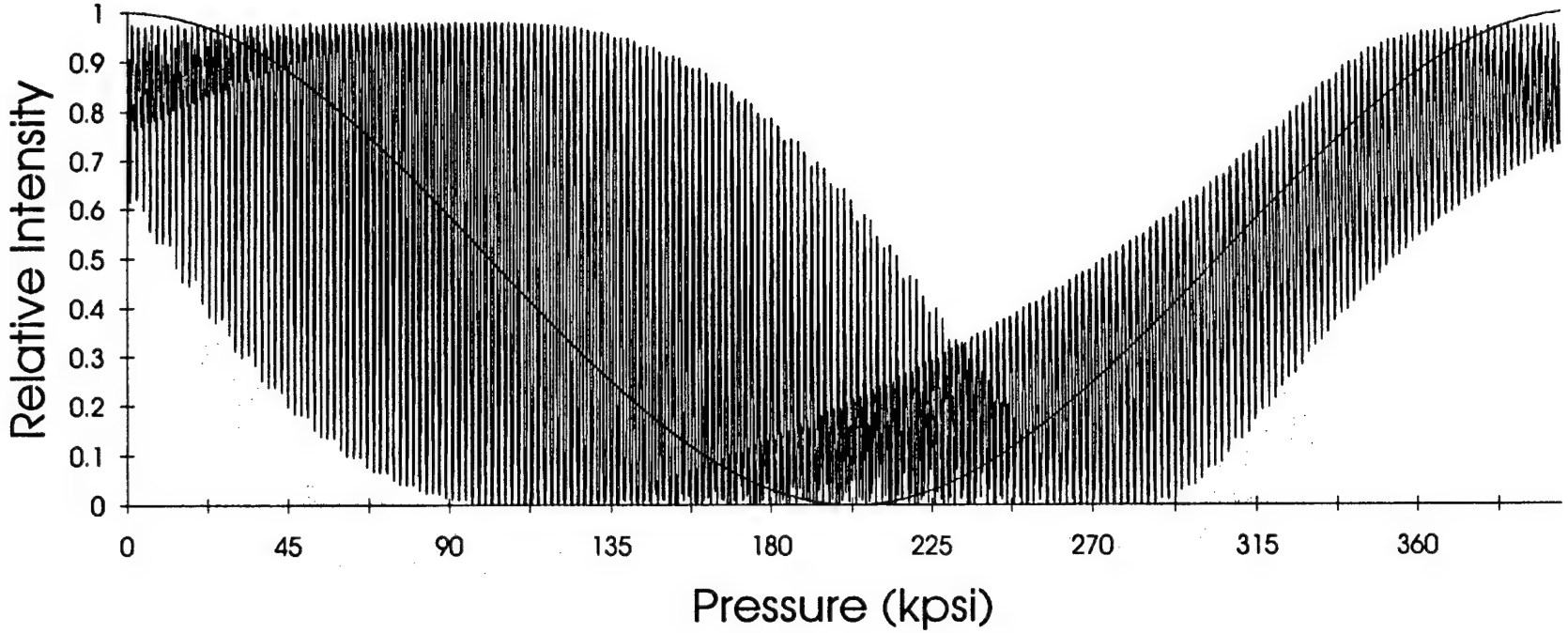

Figure A-2. Pressure-Dependent Intensity Response for the Example System With a Long Coherence Length, Narrow Band Source at 589 nm.

To observe the effect of antireflection coatings, the example system was modified by adding additional plates to represent such coatings. As a starting point, the coating was chosen to be an isotropic thin film with an index of refraction (n_c) and thickness (d) prescribed by

$$n_c = \sqrt{n_{air} n_{crystal}} \tag{A-16}$$

and

$$d = (\lambda / 4) / n_c . \tag{A-17}$$

The index of refraction of MgF_2 (1.38) is close to the optimum value (1.33) for n_c and chosen for the simulation. With this choice, it follows that d should be 0.1067 μm. The simulation was then allowed to vary d, the scale of the y-axis, and the baseline in an attempt to fit to results obtained in the absence of interference (Figure 2[a]). The results obtained in this manner are shown in Figure A-3. There is a significant reduction in the range of compression values associated with a given intensity value, but the uncertainty is still large—being of the order of 20 MPa for pressures near 345 MPa. Better results could perhaps have been achieved if a function besides equation (9) was chosen as the optimization goal, but this possibility was not explored.

To analyze the effect of employing a broad band radiation source with a non-negligible coherence length, the synthetic SLD wavelength spectrum was employed in the calculation. (Indeed, it was hoped that the interference effects produced for different wavelengths would smooth out the response.) MgF_2 was again selected as an antireflection coating—this time with a starting point thickness of 0.154 μm, and the response shown in Figure 2(b) as the optimization goal. The results, (shown in Figure A-4) are similar to the monochromatic case.

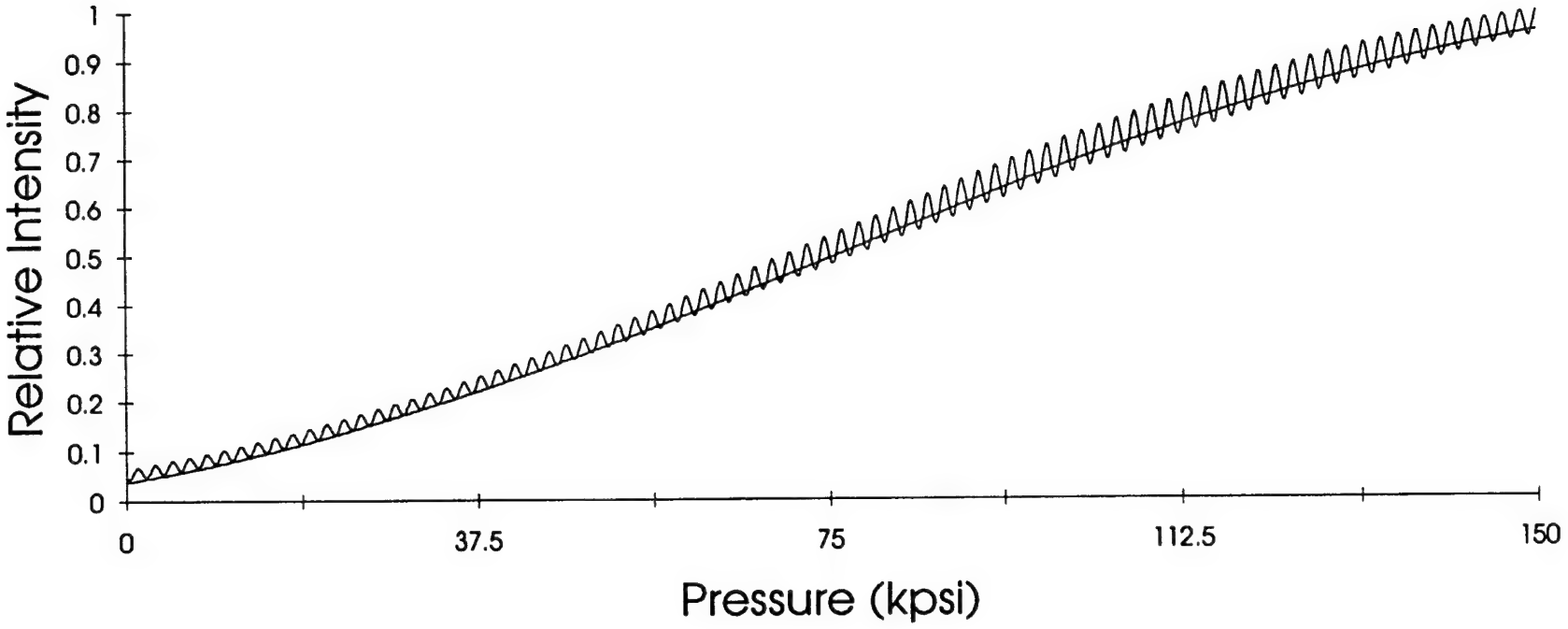

Figure A-3. Pressure-Dependent Intensity Response for the Example System With Antireflection Coatings and a Long Coherence Length, Narrow Band Source at 589 nm.

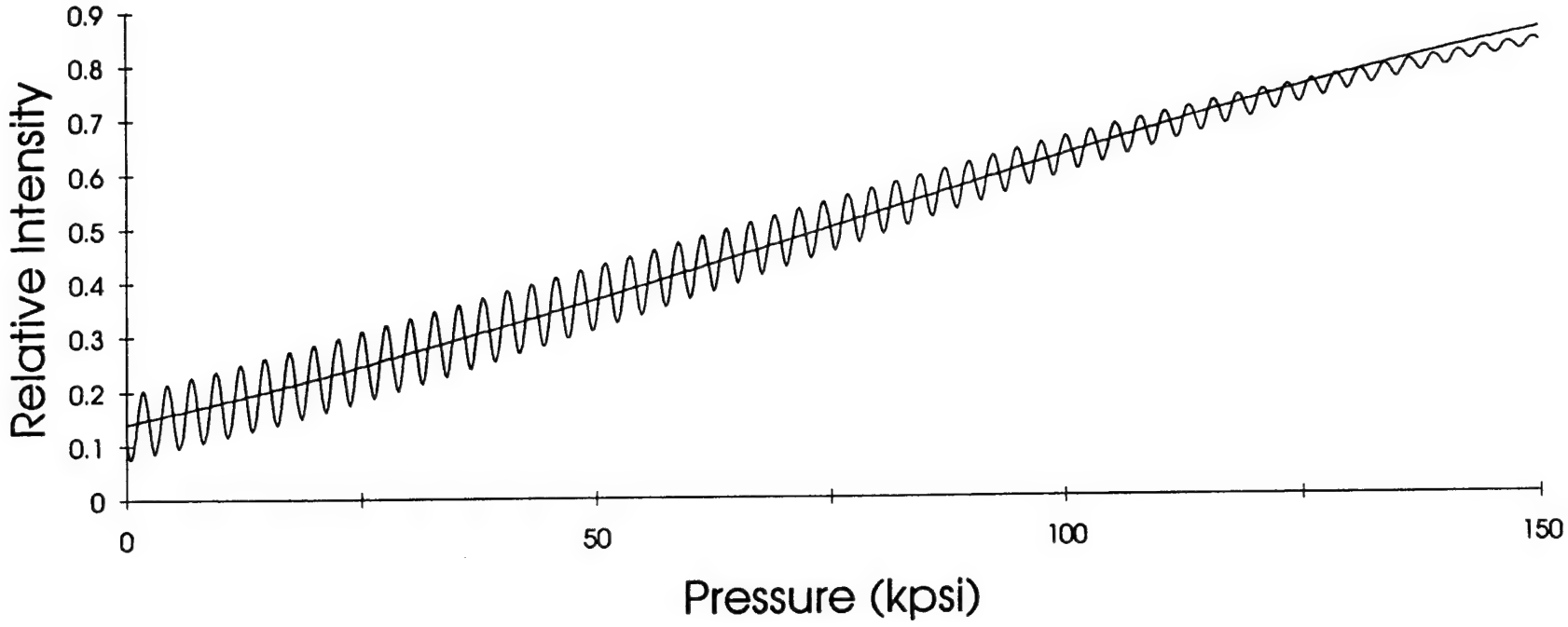

Figure A-4. Pressure-Dependent Intensity Response for the Example System With a Long Coherence Length, Broad Band Source (850 nm, 25-nm FWHM Lorentzian Distribution).

INTENTIONALLY LEFT BLANK.

NO. OF COPIES	ORGANIZATION
2	DEFENSE TECHNICAL INFORMATION CENTER DTIC DDA 8725 JOHN J KINGMAN RD STE 0944 FT BELVOIR VA 22060-6218
1	HQDA DAMO FDQ DENNIS SCHMIDT 400 ARMY PENTAGON WASHINGTON DC 20310-0460
1	CECOM SP & TRRSTRL COMMCTN DIV AMSEL RD ST MC M H SOICHER FT MONMOUTH NJ 07703-5203
1	PRIN DPTY FOR TCHNLGY HQ US ARMY MATCOM AMCDCG T M FISETTE 5001 EISENHOWER AVE ALEXANDRIA VA 22333-0001
1	PRIN DPTY FOR ACQUSTN HQS US ARMY MATCOM AMCDCG A D ADAMS 5001 EISENHOWER AVE ALEXANDRIA VA 22333-0001
1	DPTY CG FOR RDE HQS US ARMY MATCOM AMCRD BG BEAUCHAMP 5001 EISENHOWER AVE ALEXANDRIA VA 22333-0001
1	DPTY ASSIST SCY FOR R&T SARD TT T KILLION THE PENTAGON WASHINGTON DC 20310-0103
1	OSD OUSD(A&T)/ODDDR&E(R) J LUPO THE PENTAGON WASHINGTON DC 20301-7100

NO. OF COPIES	ORGANIZATION
1	INST FOR ADVNCD TCHNLGY THE UNIV OF TEXAS AT AUSTIN PO BOX 202797 AUSTIN TX 78720-2797
1	DUSD SPACE 1E765 J G MCNEFF 3900 DEFENSE PENTAGON WASHINGTON DC 20301-3900
1	USAASA MOAS AI W PARRON 9325 GUNSTON RD STE N319 FT BELVOIR VA 22060-5582
1	CECOM PM GPS COL S YOUNG FT MONMOUTH NJ 07703
1	GPS JOINT PROG OFC DIR COL J CLAY 2435 VELA WAY STE 1613 LOS ANGELES AFB CA 90245-5500
1	ELECTRONIC SYS DIV DIR CECOM RDEC J NIEMELA FT MONMOUTH NJ 07703
3	DARPA L STOTTS J PENNELLA B KASPAR 3701 N FAIRFAX DR ARLINGTON VA 22203-1714
1	SPCL ASST TO WING CMNDR 50SW/CCX CAPT P H BERNSTEIN 300 O'MALLEY AVE STE 20 FALCON AFB CO 80912-3020
1	USAF SMC/CED DMA/JPO M ISON 2435 VELA WAY STE 1613 LOS ANGELES AFB CA 90245-5500

NO. OF
COPIES ORGANIZATION

1 US MILITARY ACADEMY
MATH SCI CTR OF EXCELLENCE
DEPT OF MATHEMATICAL SCI
MDN A MAJ DON ENGEN
THAYER HALL
WEST POINT NY 10996-1786

1 DIRECTOR
US ARMY RESEARCH LAB
AMSRL CS AL TP
2800 POWDER MILL RD
ADELPHI MD 20783-1145

1 DIRECTOR
US ARMY RESEARCH LAB
AMSRL CS AL TA
2800 POWDER MILL RD
ADELPHI MD 20783-1145

3 DIRECTOR
US ARMY RESEARCH LAB
AMSRL CI LL
2800 POWDER MILL RD
ADELPHI MD 20783-1145

ABERDEEN PROVING GROUND

3 DIR USARL
AMSRL CI LP (305)

NO. OF COPIES	ORGANIZATION
1	HQDA SARD TT MR J APPEL WASHINGTON DC 20310-0103
1	HQDA SARD TT MS C NASH WASHINGTON DC 20310-0103
1	DIRECTOR US ARMY RESEARCH LAB AMSRL CP CA D SNIDER 2800 POWDER MILL RD ADELPHI MD 20783
1	COMMANDER US ARMY ARDEC AMSTA AR FSE T GORA PICATINNY ARSENAL NJ 07806-5000
3	COMMANDER US ARMY ARDEC AMSTA AR TD T PRICE V LINDNER C SPINELLI PICATINNY ARSENAL NJ 07806-5000
1	US ARMY TACOM AMSTA JSK SAM GOODMAN WARREN MI 48397-5000
2	PROJECT MANAGER SADARM PICATINNY ARSENAL NJ 07806-5000
1	COMMANDER US ARMY ARDEC F MCLAUGHLIN PICATINNY ARSENAL NJ 07806-5000
1	COMMANDER US ARMY ARDEC AMSTA CCH V E FENNELL PICATINNY ARSENAL NJ 07806-5000

NO. OF COPIES	ORGANIZATION
5	COMMANDER US ARMY ARDEC AMSTA AR CCH T S MUSALLI P CHRISTIAN R CARR N KRASNOW PICATINNY ARSENAL NJ 07806-5000
1	COMMANDER US ARMY ARDEC AMSTA CCH J DELORENZO PICATINNY ARSENAL NJ 07806-5000
2	COMMANDER US ARMY ARDEC AMSTA J HEDDERICH COL SINCLAIR PICATINNY ARSENAL NJ 70806-5000
1	COMMANDER US ARMY ARDEC AMSTA CCH P J LUTZ PICATINNY ARSENAL NJ 07806-5000
2	COMMANDER US ARMY ARDEC AMSTA AR FSA M D DEMELLA F DIORIO PICATINNY ARSENAL NJ 07806-5000
2	COMMANDER US ARMY ARDEC AMSTA AR FSA A WARNASCH B MACHAK PICATINNY ARSENAL NJ 07806-5000

NO. OF COPIES	ORGANIZATION
10	DIRECTOR BENET LABORATORIES AMSTA AR CCB C KITCHENS J KEANE J BATTAGLIA J VASILAKIS G FFIAR G D'ANDREA V MONTVORI J WRZOCHALSKI R HASENBEIN AMSTA AR CCB R S SOPOK WATERVLIET NY 12189-4050
1	COMMANDER SMCWV QAE Q B VANINA BLDG 44 WATERVLIET ARSENAL WATERVLIET NY 12189-4050
1	COMMANDER SMCWV SPM T MCCLOSKEY BLDG 25 3 WATERVLIET ARSNL WATERVLIET NY 12189-4050
1	COMMANDER WATERVLIET ARSENAL SMCWV QA QS K INSCO WATERVLIET NY 12189-4050
1	COMMANDER US ARMY ARDEC AMSMC PBM K PICATINNY ARSENAL NJ 07806-5000
1	COMMANDER US ARMY BELVOIR RD&E CTR STRBE JBC FORT BELVOIR VA 2200-5605
1	US ARMY COLD REGIONS RSRCH AND ENGRG LAB P DUTTA 72 LYME RD HANOVER NH 03755

NO. OF COPIES	ORGANIZATION
3	COMMANDER US ARMY MISSILE CMD AMSMI RD W MCCORKLE AMSMI RD ST P DOYLE AMSMI RD ST CN T VANDIVER REDSTONE ARSENAL AL 35898
2	US ARMY RSRCH OFFICE A CROWSON J CHANDRA PO BOX 1211 RESEARCH TRIANGLE PARK NC 27709-2211
2	US ARMY RSRCH OFFICE ENGRG SCIENCES DIV R SINGLETON G ANDERSON K IYER PO BOX 12211 RESEARCH TRIANGLE PARK NC 27709-2211
2	PROJECT MANAGER TANK MAIN ARMAMENT SYSTEMS SFAE AR TMA COL BREGARD K KIMKER PICATINNY ARSENAL NJ 07806-5000
1	PROJECT MANAGER TANK MAIN ARMAMENT SYSTEMS SFAE ASM TMA MD K KOWALSKI PICATINNY ARSENAL NJ 07806-5000
3	PEO FLD ARTILLERY SYSTEMS SFAE FAS PM D ADAMS T MCWILLIAMS H GOLDMAN PICATINNY ARSENAL NJ 07806-5000
2	PROJECT MANAGER AFAS D DELCOCO J SHIELDS PICATINNY ARSENAL NJ 07806-5000

NO. OF COPIES	ORGANIZATION
2	NASA LANGLEY RSRCH CTR MS 266 AMSRL VS W ELBER F BARTLETT JR HAMPTON VA 23681-0001
2	COMMANDER DARPA J KELLY B WILCOX 3701 N FAIRFAX DR ARLINGTON VA 22203-1714
2	COMMANDER WRIGHT PATTERSON AFB WL FIV A MAYER WL MLBM S DONALDSON 2941 P STREET STE 1 DAYTON OH 45433
1	COMMANDER US NSWC G 06 DAHLGREN VA 22448
1	NAVAL RSRCH LAB CODE 6383 I WOLOCK WASHINGTON DC 20375-5000
1	OFC OF NAVAL RSRCH MECH DIV CODE 1132SM YAPA RAJAPAKSE ARLINGTON VA 22217
1	NSWC CRANE DIVISION M JOHNSON CODE 20HR LOUISVILLE KY 40214-5245
1	DAVID TAYLOR RSRCH CTR SHIP STRCTRS & PRTCTN DEPT J CORRADO CODE 1702 BETHESDA MD 20084

NO. OF COPIES	ORGANIZATION
1	DAVID TAYLOR RSRCH CTR R ROCKWELL W PHYILLAIER BETHESDA MD 20054-5000
1	DEFENSE NUCLEAR AGENCY INNOVATIVE CONCEPTS DIV R ROHR 6801 TELEGRAPH RD ALEXANDRIA VA 22310-3398
1	EXPEDITIONARY WARFARE DIV N85 FRANK SHOUP 2000 NAVY PENTAGON WASHINGTON DC 20350-2000
1	OFC OF NAVAL RSRCH MR DAVID SIEGEL 351 800 N QUINCY ST ARLINGTON VA 22217-5660
1	NAVAL SURFACE WARFARE CTR CODE G30 JOSEPH H FRANCIS DAHLGREN VA 22448
3	NAVAL SURFACE WARFARE CTR CODE G32 DON WILSON CODE G32 R D COOPER CODE G32 ED WILSON DAHLGREN VA 22448
4	NAVAL SURFACE WARFARE CTR CODE G33 JOHN FRAYSSE CODE G33 ELDRIDGE ROWE CODE G33 TOM DURAN GODE G33 LAURA DE SIMONE DAHLGREN VA 22448
1	COMMANDER NAVAL SEA SYSTEMS CMD D LIESE 2531 JEFFERSON DAVIS HWY ARLINGTON VA 22242-5160
1	NAVAL SURFACE WARFARE CTR MARY E LACY CODE D4 17320 DAHLGREN RD DAHLGREN VA 22448

NO. OF COPIES ORGANIZATION

1 NAVAL SURFACE WARFARE CTR
TECH LIBRARY CODE 323
17320 DAHLGREN RD
DAHLGREN VA 22448

4 DIRECTOR
LLNB
R CHRISTENSEN
S DETERESA
F MAGNESS
M FINGER
PO BOX 808
LIVERMORE CA 94550

1 LOS ALAMOS NATIONAL LAB
D RABERN
MEE 13 MS J 576
PO BOX 1633
LOS ALAMOS NM 87545

1 LOS ALAMOS NATIONAL LAB
F ADDRESSIO
MS B216
PO BOX 1663
LOS ALAMOS NM 87545

1 LOS ALAMOS NATIONAL LAB
J REPPA MS F668
PO BOX 1663
LOS ALAMOS NM 87545

1 OAK RIDGE NATIONAL LAB
R M DAVIS
PO BOX 2008
OAK RIDGE TN 37831-6195

5 DIRECTOR
SANDIA NATL LABS
APPLIED MECHANICS DEPT
C ROBINSON
W KAWAHARA
K PERANO
D DAWSON
P NIELAN
DIVISION 8241
PO BOX 969
LIVERMORE CA 94550-0096

NO. OF COPIES ORGANIZATION

1 DIRECTOR
LLNL
M MURPHY
PO BOX 808 L 282
LIVERMORE CA 94550

3 INST FOR ADVNCD TECHNLGY
T KIEHNE
H FAIR
P SULLIVAN
4030 2 W BRAKER LN
AUSTIN TX 78759

ABERDEEN PROVING GROUND

76 DIR USARL
ATTN AMSRL CI,
C MERMAGEN 394
AMSRL CI C,
W STUREK 1121
AMSRL CI CB,
R KASTE 394
AMSRL CI S,
A MARK 309
AMSRL SL B,
P DIETZ 329
AMSRL SL BA
AMSRL SL BL,
D BELY 328
AMSRL WM P,
A HORST 390A
E SCHMIDT 390A
AMSRL WM PA,
G KELLER 390
J COLBURN
T ROSEN BERGER
A JUHASZ
W OBERLE
G WREN
C LEVERITT 390
D KOOKER 390A
AMSRL WM PB,
P PLOSTINS 390
D LYON 390

NO. OF COPIES ORGANIZATION

ABERDEEN PROVING GROUND (Cont)

AMSRL WM PC,
B FORCH 390A
R FIFER 390
R PESCE-RODRIGUEZ 390
R A BEYER
M J MCQUAID (10 CP)
K L MCNESBY
W F MCBRATNEY
M S MILLER
A W MIZIOLEK
J A VANDERHOFF
AMSRL WM PD,
B BURNS 390
W DRYSDALE 390
J BENDER 390
R KIRKENDALL 390
T ERLINE 390
D HOPKINS 390
S WILKERSON 390
D HENRY 390
R KASTE 390
L BURTON 390
J TZENG 390
R LIEB 390
G GAZONAS 390
M LEADORE 390
C HOPPEL 390
AMSRL WM PD (ALC),
A ABRAHAMIAN
M BERMAN
A FRYDMAN
T LI
W MCINTOSH
E SZYMANSKI
AMSRL WM T,
W MORRISON 309
AMSRL WM TA,
W GILLICH 390
W BRUCHEY 390
AMSRL WM TC,
K KIMSEY 309
R COATES 309
W DE ROSSET 309
AMSRL WM TD,
D DIETRICH 309
J HUFFINGTON 309
A DAS GUPTA 309

NO. OF COPIES ORGANIZATION

AMSRL WM W,
C MURPHY 120
AMSRL WM WA,
H ROGERS 394
AMSRL WM WB,
F BRANDON 120
W D'AMICO 120
AMSRL WM WC,
J BORNSTEIN 120
AMSRL WM WD,
J POWELL 120
AMSRL WM WE,
J LACETERA 120
AMSRL SE L (ALC),
D WOODBURY

1 CDR USA ATC
S WALTON

INTENTIONALLY LEFT BLANK.

REPORT DOCUMENTATION PAGE

Form Approved
OMB No. 0704-0188

1. AGENCY USE ONLY *(Leave blank)*	2. REPORT DATE	3. REPORT TYPE AND DATES COVERED
	August 1997	Final, May 94 - Jan 97

4. TITLE AND SUBTITLE

An Optically Based Pressure Measurement Approach for Interior Ballistic Testing

5. FUNDING NUMBERS

PR: 1L161102AH43

6. AUTHOR(S)

Michael J. McQuaid

7. PERFORMING ORGANIZATION NAME(S) AND ADDRESS(ES)

U.S. Army Research Laboratory
ATTN: AMSRL-WM-PC
Aberdeen Proving Ground, MD 21005-5066

8. PERFORMING ORGANIZATION REPORT NUMBER

ARL-TR-1472

9. SPONSORING/MONITORING AGENCY NAMES(S) AND ADDRESS(ES)

10.SPONSORING/MONITORING AGENCY REPORT NUMBER

11. SUPPLEMENTARY NOTES

12a. DISTRIBUTION/AVAILABILITY STATEMENT

Approved for public release; distribution is unlimited.

12b. DISTRIBUTION CODE

13. ABSTRACT *(Maximum 200 words)*

This report describes a recent patent disclosure for obtaining an optically based measurement of pressure. The concept, which utilizes pressure-induced changes in polarization to modulate intensity, incorporates a means of addressing a universal shortcoming of optically based techniques—namely, temperature sensitivity. The invention has application for any pressure regime, but will be particularly advantageous for electrically or physically harsh environments. Embodiments of this concept may provide a suitable replacement for piezoelectric-based pressure transducers used in the testing of advanced gun propulsion system concepts. A design for a transducer that could be used to measure pressure from 0 to 1 GPa is provided as an example, and issues related to building a prototype for use in ballistic testing are identified and discussed.

14. SUBJECT TERMS

pressure measurement, interior ballistics, RLPG

15. NUMBER OF PAGES

34

16. PRICE CODE

17. SECURITY CLASSIFICATION OF REPORT	18. SECURITY CLASSIFICATION OF THIS PAGE	19. SECURITY CLASSIFICATION OF ABSTRACT	20. LIMITATION OF ABSTRACT
UNCLASSIFIED	UNCLASSIFIED	UNCLASSIFIED	UL

INTENTIONALLY LEFT BLANK.

USER EVALUATION SHEET/CHANGE OF ADDRESS

This Laboratory undertakes a continuing effort to improve the quality of the reports it publishes. Your comments/answers to the items/questions below will aid us in our efforts.

1. ARL Report Number/Author ARL-TR-1472 (McQuaid) Date of Report August 1997

2. Date Report Received _____

3. Does this report satisfy a need? (Comment on purpose, related project, or other area of interest for which the report will be used.) _____

4. Specifically, how is the report being used? (Information source, design data, procedure, source of ideas, etc.) _____

5. Has the information in this report led to any quantitative savings as far as man-hours or dollars saved, operating costs avoided, or efficiencies achieved, etc? If so, please elaborate. _____

6. General Comments. What do you think should be changed to improve future reports? (Indicate changes to organization, technical content, format, etc.) _____

CURRENT ADDRESS

_____
Organization

_____
Name E-mail Name

_____
Street or P.O. Box No.

_____
City, State, Zip Code

7. If indicating a Change of Address or Address Correction, please provide the Current or Correct address above and the Old or Incorrect address below.

OLD ADDRESS

_____
Organization

_____
Name

_____
Street or P.O. Box No.

_____
City, State, Zip Code

(Remove this sheet, fold as indicated, tape closed, and mail.)
(DO NOT STAPLE)

DEPARTMENT OF THE ARMY

OFFICIAL BUSINESS

NO POSTAGE
NECESSARY
IF MAILED
IN THE
UNITED STATES

BUSINESS REPLY MAIL
FIRST CLASS PERMIT NO 0001,APG,MD

POSTAGE WILL BE PAID BY ADDRESSEE

DIRECTOR
US ARMY RESEARCH LABORATORY
ATTN AMSRL WM PC
ABERDEEN PROVING GROUND MD 21005-5066